Efficient synthesis, crystallographic study, antimicrobial activity and in silico studies of novel bioactive α-aminophosphonates based on pyridine moiety

Ismahene Grib, Malika Berredjem, Seif-Eddine Djouad, Chahrazed Benzaid, Khadidja Otmane Rachedi, Rania Bahadi, Lina Manel Djendi, Malika Ibrahim-Ouali, Sofiane Bouacida, Khaldoun Bachari, et al.

Efficient synthesis, crystallographic study, antimicrobial activity and *in silico* studies of novel bioactive α-aminophosphonates based on pyridine moiety

Ismahene Grib [a], Malika Berredjem [a,*], Seif-Eddine Djouad [a,b], Chahrazed Benzaid [a,c], Khadidja Otmane Rachedi [a,d], Rania Bahadi [a], Lina Manel Djendi [a], Malika Ibrahim-Ouali [e], Sofiane Bouacida [f,g], Khaldoun Bachari [h], Yacine Laichi [h], Christelle Marminon [i], Marc LE Borgne [i], Radia Bouasla [a]

[a] *Laboratory of Applied Organic Chemistry, Synthesis of Biomolecules and Molecular Modelling Group, Faculty of Sciences, Department of Chemistry, Badji-Mokhtar - Annaba University, Box 12, Annaba 23000, Algeria*
[b] *Laboratory of Therapeutic Chemistry of Hospitalo-University Center Benfis Touhami, Batna, Algeria*
[c] *Laboratory of Microbiology and Molecular Biology, Badji-Mokhtar - Annaba University, Box 12, Annaba 23000, Algeria*
[d] *Université El-Tarf, Faculté des sciences et de la technologie, El Taref BP 73, Algeria*
[e] *Aix Marseille Univ, CNRS, Centrale Marseille, iSm2, Marseille, France*
[f] *Département de Sciences de la Matière, Université Oum El Bouaghi, Oum El Bouaghi 04000, Algeria*
[g] *Unité de Recherche de Chimie de l'Environnement et Moléculaire Structurale, Université Frères Mentouri Constantine*
[h] *Centre de Recherche Scientifique et Technique en Analyses Physico-chimiques (CRAPC), BP384, Bou-Ismail, Tipasa RP 42004, Algeria*
[i] *Small Molecules for Biological Targets Team, Centre de Recherche en Cancérologie de Lyon, Centre Léon Bérard, Institut National de la Santé et de la Recherche Médicale (INSERM) 1052, Centre National de la Recherche Scientifique (CNRS) 5286, Université Claude Bernard Lyon 1, Lyon 69373, France*

Keywords:
α-Aminophosphonate
X-ray diffraction
DFT
Molecular docking
Antimicrobial activity

This study articulates the synthesis, spectroscopic characterization, antimicrobial evaluation, theoretical calculations, and molecular docking analysis of a novel α-aminophosphonates derived from aminopyridine as potential antibacterial pharmacophore. The structures of all compounds was established using FTIR, ^{1}H, ^{13}C, ^{31}P NMR spectroscopy. A single crystal of the studied compound **3g** was selected for X-ray diffraction analysis, it crystallizes in the monoclinic crystal system with P 21/n space group. Theoretical studies based on density functional theory (DFT) at the B3LYP /6-31G (d, p) level of theory was utilized to investigate the stability and electronic properties electronic of the studied α-aminophosphonates. The ADME/toxicity analyzes carried out by Swiss ADME and OSIRIS software show that all synthesized molecules exhibited good pharmacokinetics, bioavailability and had no toxicity profile.

1. Introduction

The search for new antimicrobial molecules is crucial to combat the rising antibiotic resistance and to develop effective treatments for bacterial, viral, and fungal infections.

α-Aminophosphonic acid derivatives are recognized as biologically active molecules due to their structural resemblance to natural α-amino acids [1–4]. In particular, a number of α-aminophosphonate derivatives have found applications as agrochemicals [5,6], antimicrobial [7–8], antioxidant [9–10], anticancer agents [11], antitumor [12], antiviral [13] and antitubercular [14] (Fig. 1).

The incorporation of a phosphorus-containing group with a heterocyclic fragment has yielded heterocyclic phosphonates with noteworthy chemical and biological properties [15–18] (Fig. 2). Medicinal chemistry and molecular modeling techniques are employed to create hybrid compounds that incorporate the key features of each pharmacophore. These new hybrid biomolecules are then tested in vitro and in vivo to assess their efficacy, selectivity, and toxicity.

The development of new drugs by combining two pharmacophores involves creating chemical compounds that integrate the active features of two distinct groups of molecules, or pharmacophores. This approach aims to leverage the positive pharmacological properties of each

pharmacophore to create a more effective drug, potentially with fewer side effects.

The significance of α-aminophosphonate in the biological and chemical field has led to the development of numerous synthetic methods of novel derivatives. Consequently, there is a significant demand for the development of efficient synthesis protocols to facilitate the production of these compounds.

Due to the aforementioned factors and as a continuation of our work in developing a new series of phosphonates [19–21], we have easily synthesized a new series of hybrid analogs of aminophosphonates containing a pyridine core. The newly synthesized derivatives were evaluated for their antimicrobial activity against bacterial and fungi stains: *S. aureus, E. cloacae, Moraxella lacunat P. aeruginosa, C. albicans, C. Krusei* and *C. lusitaniae.* The pharmacokinetics and toxicity of these compounds were investigated using ADME-SAR, SwissADME, and molinspiration.

2. Results and discussion

2.1. Synthesis

In recent years [22–26], solvent-free reactions and the use of ultrasound have gained much attention since these methods was valuable not only for ecological and economic reasons but also for operational simplicity and to obtain high yields of products. Emphasis was also done toward the development of clean and green chemical processes. Due to this reason a library of α-aminophosphonates were synthesized via three-component Kabachnik-Fields reaction by use of different aromatic aldehydes (1 equiv), 2-amino pyridine (1 equiv) and trimethyl phosphite (1.2 equiv), under ultrasonic irradiation at room temperature and solvent-free, catalyst-free conditions during 10–20 min. After that, the solid product was recrystallized in diethyl ether and dried at room temperature in excellent yields.

The α-aminophosphonate derivatives are represented by structure 3 in the general (Scheme 1) and (Table 1).

2.2. Crystallographic study

Single-crystal X-ray diffraction studies reveal that **3g** is composed of a 3D framework connected with hydrogen bond interactions. Structural resolution revealed that the asymmetric unit consists of one molecule of (dimethyl (naphthalen-1-yl(pyridin-2-ylamino)methyl)phosphonate, **3g**), which crystallizes in the Triclinic crystal system with *P -1* space group (Table 2). The ellipsoid Plot (ORTEP) [27] illustration of one representative molecular structure of **3g** is exposed in (Fig. 3). The dihedral angles formed between double phenyl rings and pyridine ring in the asymmetric unit is 52.53°.

The crystal packing can be described as alternating double layers parallel to (001) plane along the c axis (Figs. 4 and 5), which are connected together with N-H...O hydrogen bonds along the c axis (Fig. 5, Table 3).

In these layers, the arrangement of each molecule induces a π–π staking intermolecular interactions. The shortest centroid–centroid distance is 4.7139(11) Å between phenyl rings.

The crystal structure is also supported by intramolecular hydrogen bond of C-H…N and weak intermolecular interactions of C-H... π interactions.

2.3. Antimicrobial activity

Based on these results, it was observed in Fig. 6 very interesting antimicrobial activity when compared with the scale presented by Billberck et *al.* [28], where there are three levels of activity: resistant (D < 6 mm), intermediate (13 mm - 6 mm D) and sensitive (D > 13 mm).

Despite the known antibiotic resistance of *Staphylococcus aureus* (a Gram-positive bacterium) [29], molecules **3a, 3b** and **3d** inhibited its growth, with a zone of inhibition ranging from 19 to 14 mm in diameter. Gram-positive bacteria are known for their thick cell walls, due to the presence of a peptidoglycan layer that makes them resistant to the action of treatments [30]. This resistance was also observed with ampicillin, which was our positive control.

For Gram-negative bacteria, *Pseudmonas aeruginosa* was the most sensitive germ; with DZIs ranging from 34 mm for 3f to 16 mm for 3c, this bacterium also proved sensitive to all the molecules tested, with the exception of 3b.

The same applies to *Enterobacter cloacae*, with a DZI ranging from 28 to 16. *Klebsiella pneumoniae*, on the other hand, proved more resistant to the action of synthesized α-aminophosphonate, although the DZIs were 24 mm for 3d and 20 mm for 3f.

In terms of fungal growth inhibition, we found moderate activity, with absolute resistance from *Candida krusei*, while *Candida albicans* was only sensitive to the action of 3b with a DZI of 15 mm.

Our results were also confirmed by the determination of the minimum inhibitory concentration (MIC). shown in (Table 4).

The results showed that these compounds have moderate MICs ranging from 32 to 128 μg/mL. the MIC results for ampicillin used as standard treatment in our study remain relatively higher than those observed with our molecules.

MIC values are moderate and may suggest a Dose/Response study to

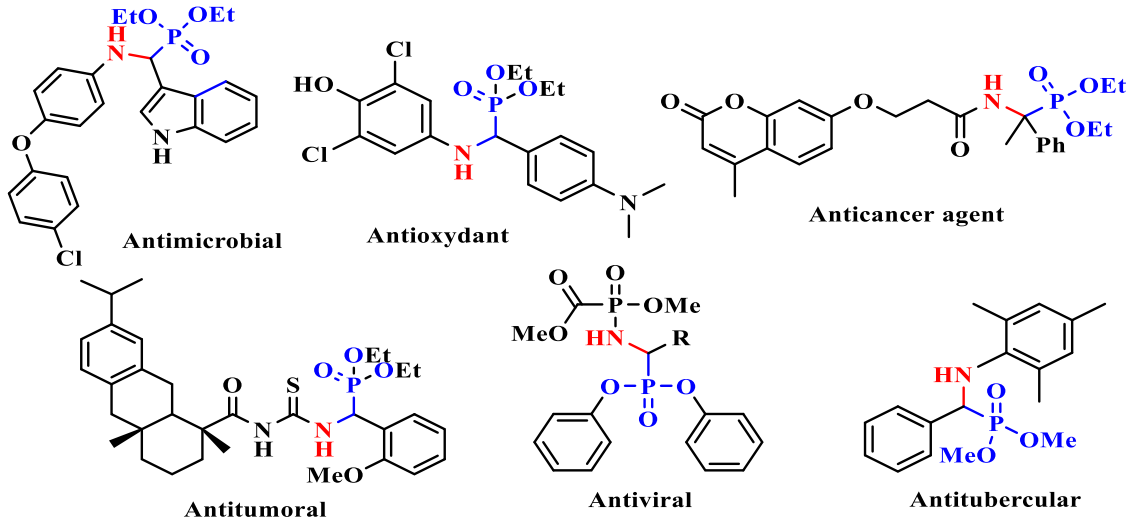

Fig. 1. Some examples of biologically active α-aminophosphosphonate derivatives.

better assess the antimicrobial effect of our molecules.

2.4. Molecular docking analysis

Infections with Pseudomonas aeruginosa (PA) are notoriously challenging to treat and often come with the development of antimicrobial resistance (AMR) [31].This resistance has become a global health concern, to the extent that the World Health Organization (WHO) has classified carbapenem-resistant Pseudomonas aeruginosa (PA) as one of the highest-priority pathogens to control.

In the present study, we employed an innovative approach known as antivirulence or pathoblocking, targeting a specific regulatory network that controls virulence, called quorum sensing (QS) [32]. Quorum sensing (QS) is a major signaling mechanism that directly contributes to biofilm formation. Biofilms are structured communities of microorganisms that are notoriously resistant to conventional treatments [32–34].

In this molecular docking study, we elucidated the mechanism of pharmacological inhibition of the quorum-sensing regulator MvfR (PqsR) of *P. aeruginosa*. In doing so, we utilized α-aminophosphonate derivatives to disrupt biofilm formation and enhance the biofilm's sensitivity to antibiotics. This innovative approach could represent a significant advancement in combating the persistence of *P. aeruginosa* in various environments, bypassing its formidable resistance to traditional antimicrobial treatments [32–34].

To elucidate the binding mode and mechanism of action of novel α-aminophosphonates, we investigated the binding domain of the triazolo-pyridine inverse agonist A ligand with the biological target PqsR (MvfR) [35] (Fig. 7).

The inverse agonist A, characterized by a triazolo-pyridine ligand, formed a hydrogen bond with the THR 265 residue through its nitrogen side amine function. Additionally, hydrophobic interactions were established involving residues ALA 102, ALA 168, THR 256, ILE 149, ILE 186, ILE 236, ILE 263, and PHE 221, as illustrated in (Fig. 7) [35].

Validation of our docking methodology was achieved with an RMSD value below 2 Å [21], confirming the accuracy of our predictions regarding the ligand-protein conformation, as depicted in (Fig. 8).

Compounds **3c, 3d**, and **3g** demonstrated significant results, with a binding free energy ranging from -6.42 to -6.67 kcal/mol, promoting substantial stability in the active site of the quorum-sensing regulator MvfR (PqsR) of *P. aeruginosa*. (Table 5).

In all α-aminophosphonates derivatives, a hydrogen bond is formed via the NH binding group, except for molecule **3b** (Figs. 9–15). Compound **3f**, characterized by the presence of the phenol group, facilitates the formation of an additional second hydrogen bond (Fig. 14).

2.5. DFT study

2.5.1. Optimization Geometry

The studied molecule's optimized structures by DFT B3LYP/6-31G (d,p) are depicted in (Fig. 16).

The highest occupied molecular orbital (HOMO) and the lowest unoccupied molecular orbital (LUMO) are defined as frontier molecular orbitals, they have a crucial role in the molecule's stability from a chemical point of view [25,36-38]. The HOMO corresponds to the electron donor orbital while the LUMO corresponds to the electron acceptor orbital [39,40]. Their energies are used to better understand the molecules' chemical reactivity, calculating the global reactivity descriptors as shown [41–44] in (Table 6).

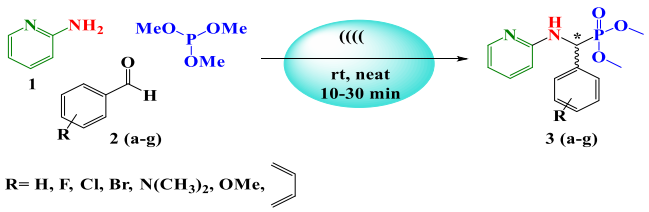

Scheme 1. Synthesis of new series of α-aminophosphonate derivatives under ultrasonic irradiation.

The quantum descriptors such as energy level (HOMO, LUMO), gap energy (ΔE_{gap}), total energy (E) and dipolar moment (DM) as well as the global reactivity descriptors are calculated and listed in (Table 7).

According to the table of results, we can notice that the compound **(3g)** is the most reactive compared with the other studied compounds because of its lower value of Eap and hardness (η). Its higher electrophelicity value (ω) confirms that it is a good electrophile.

2.5.2. Frontier molecular orbitals (FMOs) analysis and molecular electrostatic potential surface (MESP)

The frontier molecular orbitals' representation shows that the HOMO molecular orbitals of all studied compounds are distributed over the heteroatom region, except the halogens (F, Cl and Br) as well as the nitrogen atoms of compound **(3e)**.

The prediction of titled molecules' electron density localization, in addition the electrophilic and nucleophilic attacks has been carried out by the molecular electrostatic potential surface (MESP). It is frequently used as a reactivity map with the aim of explaining hydrogen-bonding interactions, and foresee the organic molecules' high electron density regions. On the MESP the different colors plot concord to the various values of electrostatic potential, the red and blue regions depicts respectively the maximum electrophilic and nucleophilic reactivity, the zero potential corresponds to the green region. The intermediate potential situated between the green and red regions is presented by the yellow and orange regions. As shown in (Fig. 17), the red region for all studied compounds corresponds to the oxygen atom of phosphine oxide.

2.5.3. Vibrational study

A vibrational study of the most reactive compound **3g** has been carried out. The vibration frequencies have been calculated by B3LYP / 6 31G (d,p) method. The Principal IR bands are given in the table below and compared with the experimental bands. This table shows that the DFT calculated IR frequency are well correlated to the experimental

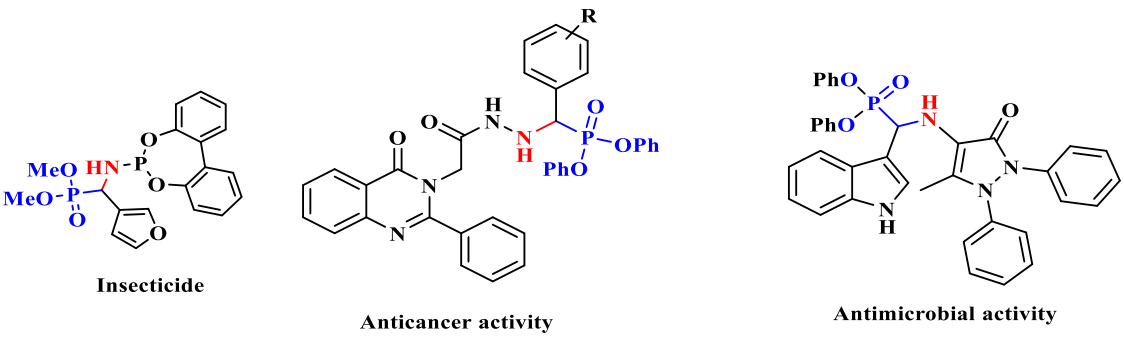

Fig. 2. Bioactive α-aminophosphonate containing heterocyles moiety.

Table 1
The physicochemical characteristics of novel α-aminophosphonates **3a-3g**.

Entry	Compound	Time (min)	Yield (%)	m.p. (°C)
3a	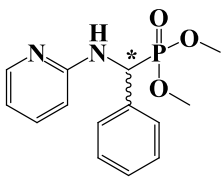	10	93	160-162
3b	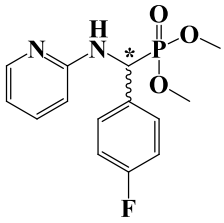	10	90	181-183
3c	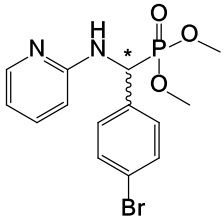	10	90	178-180
3d	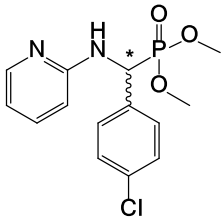	10	87	179-181
3e	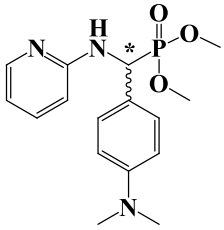	15	73	166-168
3f	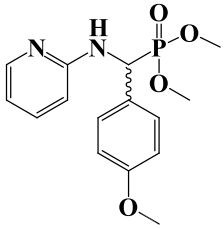	10	88	158-160
3g	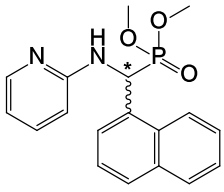	20	70	158-160

Table 2
Crystallographic data and refinement parameters for **3g**.

Formula	C_{18}	Absorption	1.539
Formula weight	$H_{19}N_2O_3P$	coefficient (mm^{-1})	360
Crystal habit,	392.42	F(000)	0.08×0.10×0.16
color	Prism,	Crystal size (mm)	4.216- 76.761
Crystal system	Colorless	θ range for data	20951
Space group	Triclinic	collection (°)	3660
a (Å)	*P -1*	Reflections collected	0.0341
b (Å)	7.9400(6)	Independent	3262
c (Å)	10.9449(8)	reflections	219
α (°)	11.7957(6)	R_{int}	1.044
β (°)	62.781(6)	Reflections with I ≥	R_1=0.0366,
γ (°)	82.080(6)	2σ(*I*)	wR_2=0.1038
Volume ($Å^3$)	74.848(7)	R_1=0.0409,	
Z, Z'	879.68(12)	parameters	wR_2=0.1080
Density	2, 2	Goodness-of-fit on F^2	0.228, -0.308
(calculated, g	1.292	Final R indices [I ≥	CCDC 2300310
cm^{-3})		2σ(*I*)]	
		R indices [all data]	
		Largest difference	
		peak and hole ($Å^{-3}$)	
		CCDC deposition no.	

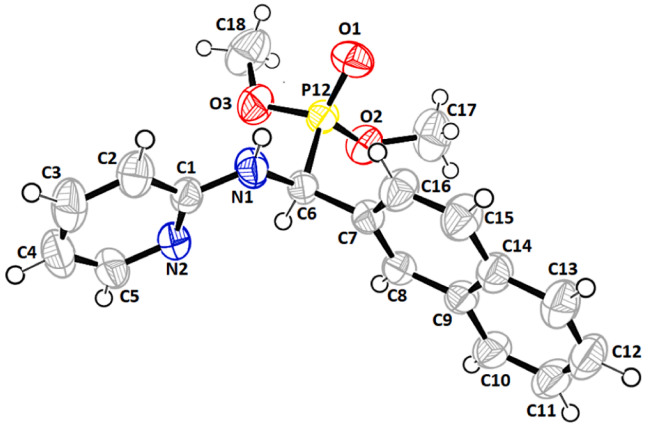

Fig. 3. Ortep diagram of compound 3g Displacement ellipsoids are drawn at the 50% probability level. H atoms are represented as small spheres of arbitrary radius.

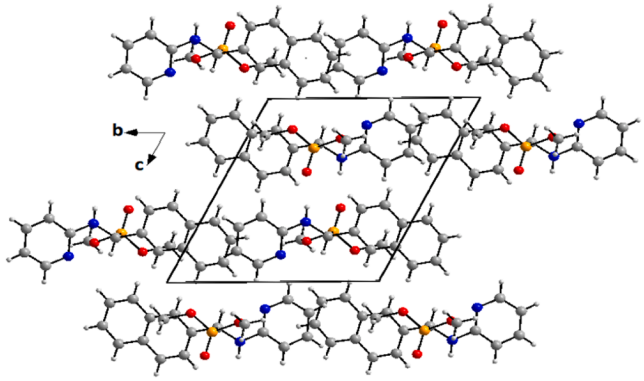

Fig. 4. Diagram packing of 3g viewed along the a axis showing double layers parallel to (001) plane along the a and c axis.

values.

2.6. ADMET predictions

The ADMET prediction, which indicates the compound's absorption, distribution, metabolism, excretion and toxicity, is very useful crucial

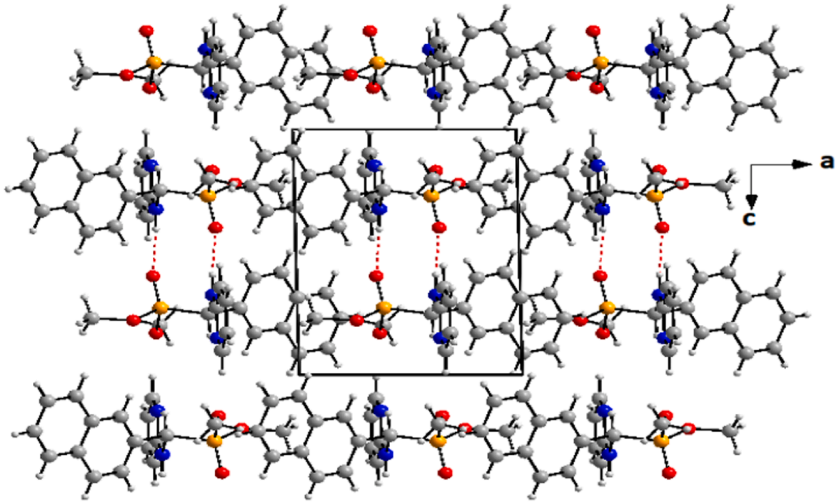

Fig. 5. Diagram packing of 3g viewed along the b axis showing N-H...O (dashed line in red) hydrogen bonds interactions.

Table 3
Distances (Å) and angles (°) of hydrogen bond for **3g**.

Compound 3g					
D–H…A	*d*(D–H)	*d*(H…A)	*d*(D–A)	D–H–A	Symmetry
N1-H1…O1	0.86	2.01	2.8697(16)	172.0	1-x,1-y,1-z
C6-H6…N2	0.98	2.28	2.764(2)	109.0	x,y,z

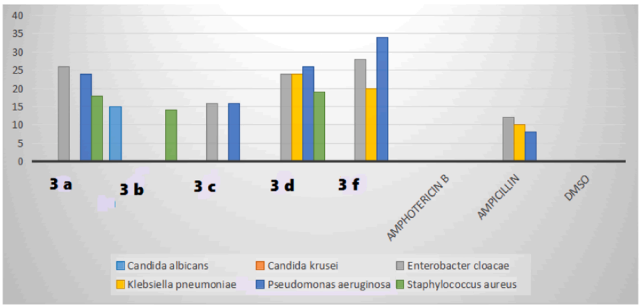

Fig. 6. Antimicrobial results of synthesized compounds Zone of inhibition (DZI :mm).

approach to discover and development drug [45,46]. It helps to the prospective compounds' identification in the early steps and moderate the potential for harmful effects in the clinical trials' time by optimizing (ADMET) drug properties.

Poor candidate's properties indicates a high risk of its failure, in this case, it may become a less than ideal medication. The ideal oral drug must follow the Lipinski's five rules [47,48]. (Table 8), and answer several requirements (Table 9).

The studied compounds' ADME outcomes are depicted in (Table 10). According to this table the studied compounds satisfy the lipinski's five rule. The (iLOGP) and Log K_p parameters are closed. In addition the target compounds are regarded as a promising therapeutic candidate, due to its high values of Log Kp > - 6.84 cm/s or skin permeability, gas trointestinal absorption (GI for short), moreover, the Blood Brain Barrier (BBB, for short) penetration.

The studied compounds' oral bioavailability radar is illustrated in (Fig. 18). As shown the values of all compound's parameters included in the good bioavailability's desired, except the unsaturation parameter, which fixes that the under study molecules can ensure the pharmacokinetic requirements necessary for the drug-like compounds' comportment, Confirming the quality of the studied compounds' oral bioavailability.

A studied compounds' toxicity prediction has been evaluated employing the free Osiris web service [49] and the outcomes are listed in (Table 11).

The topological polar surface area (algoriPSA) is used to predict the good drug absorption in the intestine (TPSA < 140 $Å^2$) and blood-brain barrier penetration (TPSA < 60 $Å^2$) [50]. The TPSA values of all studied compounds are less than 140 $Å^2$, so, these latter have good intestinal absorption. The toxicity risk prediction shows that all studied compounds are irritating and not effective for reproduction, however, they are not mutagenic and not tumorigenic, except the compounds **(3e** and **3g)**. These compounds have the close values to DL and DS, except the compound **3g**.

3. Experimental section

3.1. Chemistry

All chemicals and solvents were purchased from common

Table 4
The minimal inhibitory concentration (MIC: µg/mL) of the tested compounds.

	Strains					
Molecules	*P.aeruginosa*	*E.cloacae*	*K.pneumoniae*	*S.aureus*	*C.krusei*	*C.albicans*
3a	64	64	/	128	/	/
3b	/	/	/	128	/	128
3c	128	128	/	/	/	/
3d	64	64	128	128	/	/
3f	32	64	128	128	/	/
Ampicillin	+128	128	+128	R	/	/
Amphotericin b	/	/	/	/	R	R

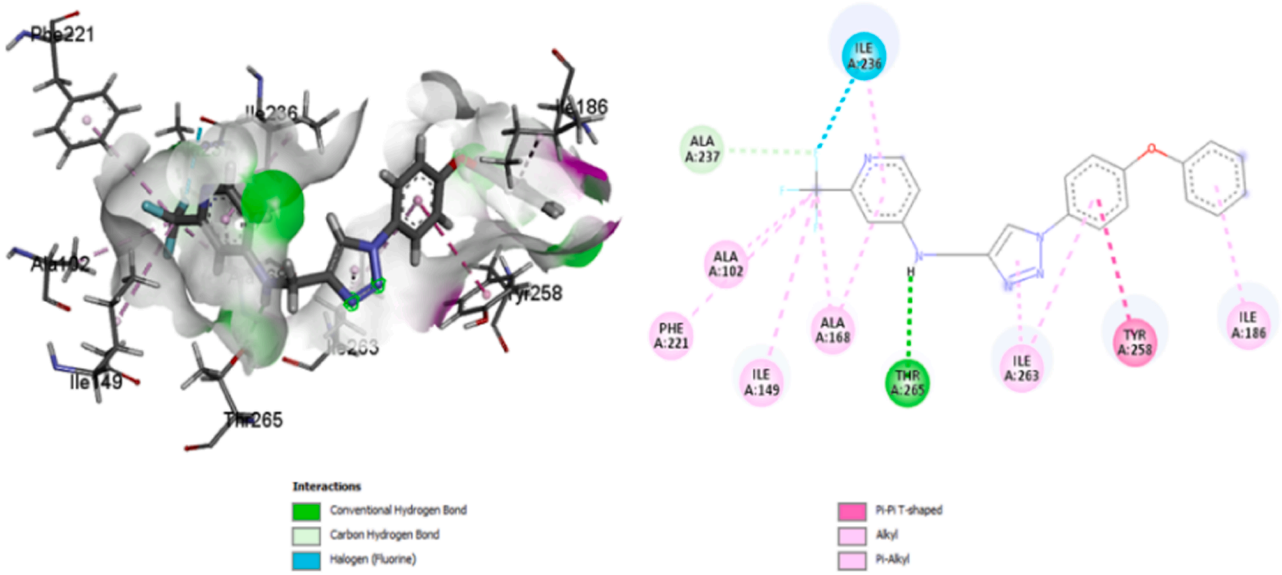

Fig. 7. Cocrystal structure of compound triazolo-pyridine inverse agonist A in complex with PqsR91-319 (PDB ID: 6YIZ) at a resolution of 2.15 Å.

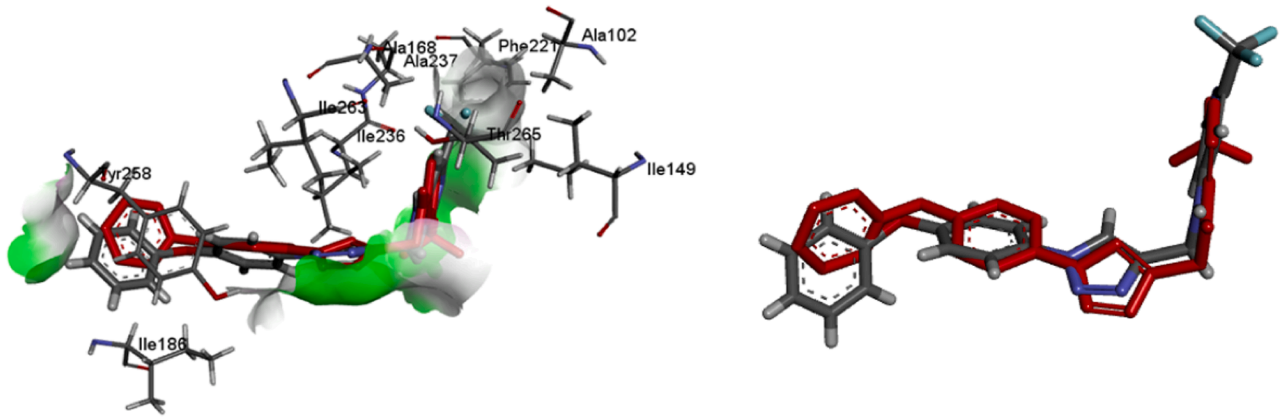

Fig. 8. Re-docking of the co-crystallized ligand triazolo-pyridine inverse agonist A (PDB ID: 6YIZ).

commercial sources and were used as received without any further purification.

Melting points were determined in open capillary tubes on an Electro thermal apparatus and uncorrected. IR spectra were recorded on a Perkin-Elmer FT-600 spectrometer. Proton nuclear magnetic resonance was determined with a 360 WB or AC 250-MHzBruker spectrometer using $CDCl_3$ and DMSO-*d6* as a solvent and TMS as an internal standard.

Chemical shifts are reported in δ units (ppm). All coupling constants (*J*) are reported in Hertz. Multiplicity is indicated by one or more of the following: s (singlet), d (doublet), t (triplet), dd (doublet of doublet), dt (doublet of triplet), and m (multiplet). Electron ionization mass spectra (30 ev) were recorded in positive mode on a Water Micro Mass ZQ. All reactions were monitored by TLC on silica Merck h60 F254 (Art. 5554) percolated aluminum plates and were developed by spraying with ninhydrin solution.

3.2. X-ray measurement

A single crystal of the studied compound **3g** was selected for X-ray diffraction analysis. The crystal was kept at 296 K during data collection., on a Agilent SUPER NOVA diffractometer, CCD area detector (ATLAS2) equipped with a mirror monochromatized Cu Kα radiation (λ= 1.54184 Å). The reported structures were solved by direct methods with SIR2002 [51] to locate all the non-H atoms which were refined anisotropically with SHELXL97 [52] using full matrix least squares on F^2 procedure from within the WinGX [53] suite of software used to prepare material for publication. All the H atoms were located in difference Fourier maps and were placed in the calculated positions and constrained to ride on their parent atoms.

The crystallographic data and experimental details for structural analysis are summarized in (Table 12). Drawings of molecules were produced with the program ORTEP-3 and Diamond [27,54].

3.3. Antimicrobial activity

3.3.1. Microorganisms and media

Microbial strains were supplied by the Harkat Medical Analysis Laboratory -Annaba-Algeria. It's about: fungi: *Candida albicans, Candida krusei* and bacteria: *Enterobacter cloacae, Klebsiella pneumoniae Pseudomonas aeruginosa* and *Staphylococcus aureus.*

These strains were used to test the antimicrobial activity of the new synthesized α-aminophosphonate. Bacteria were grown in Luria Bretani (LB) broth and on Petri dishes containing LB medium at 37°C for and yeasts grown in Sabouraud broth and on Petri dishes containing Sabouraud medium at 37°C. The specific growth rate (μ) was measured using a microplate reader at 600nm in Muller Hinton medium for bacteria and

Table 5
Ranking of novel α-aminophosphonates (**3a-3g**) and Ligand triazolo-pyridine after docking study.

N	protein	Compound	RMSD	Free Energy of Binding	Inhibition Constant, Ki	Amino acids involved in interactions	
1	**PqsR**	**Ligand triazolo-pyridine**	**1.95**	**7.19**	**5.83 uM**	**liaison hydrogen** hydrophobic interactions	THR 265 ALA 102, ALA 168, THR 256, ILE 149, ILE 186, ILE 236 and PHE 221
2	**PqsR**	**3a**	**0.00**	**-6.04**	**37.65 uM**	liaison hydrogen hydrophobic interactions	LEU 207 ALA 102, ILE 149, ILE 236, LEU 208 and PRO 129
3	**PqsR**	**3b**	**0.00**	**-5.52**	**90.48 uM**	liaison hydrogen hydrophobic interactions	LEU 197 ALA 102, ALA 168, ILE 149, ILE 236 and PRO 238
4	**PqsR**	**3c**	**0.00**	**-6.54**	**16.14 uM**	liaison hydrogen hydrophobic interactions	LEU 207 ILE 263, ILE 236, LEU 208 and LEU 207
5	**PqsR**	**3d**	**0.00**	**-6.42**	**19.67 uM**	liaison hydrogène hydrophobic interactions	ILE 236 ALA 102, ALA 168, ILE 263, ILE 149, LEU 208 and PRO 238
6	**PqsR**	**3e**	**0.00**	**-5.66**	**71.13 uM**	liaison hydrogen 7hydrophobic interactions	LEU 207 ILE 263, ILE 236, LEU 208 and LEU 207
7	**PqsR**	**3f**	**0.00**	**-6.01**	**39.04 uM**	liaison hydrogen hydrophobic interactions	LEU 207 LEU 197 MET 224, ILE 236, LEU 208 and LEU 207
8	**PqsR**	**3g**	**0.00**	**-6.67**	**12.85 uM**	liaison hydrogen hydrophobic interactions	LEU 207 PRO 210, ILE 236, LEU 208

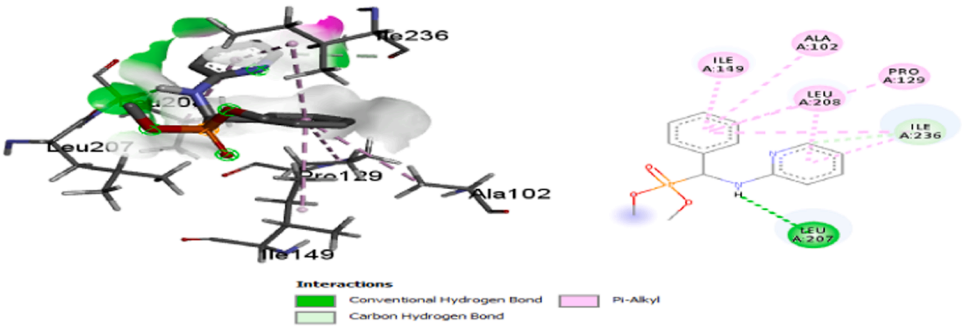

Fig. 9. Binding site structure of compound 3a- PqsR91-319.

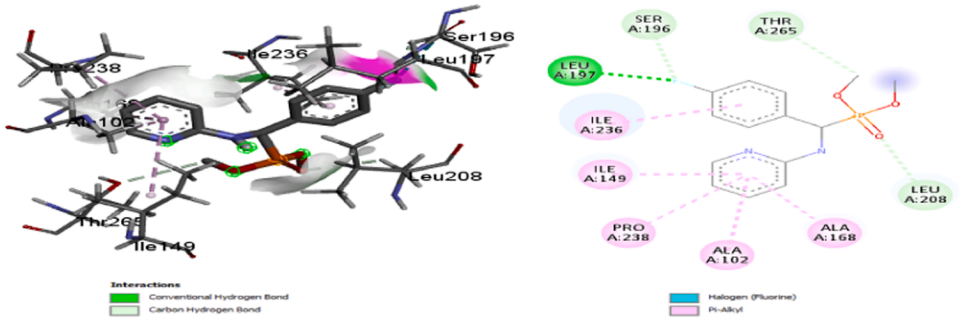

Fig. 10. Binding site structure of compound 3b- PqsR91-319.

Saouraud medium for yeasts. Used for testing antimicrobial activity and determining MIC and MBC.

3.3.2. Antimicrobial test

The agar-well diffusion method [55] was used to determine the antimicrobial activity of the neosynthesized molecules. Ampicillin and amphotericin b were used as positive reference standards to determine bacterial and yeast susceptibility respectively. DMSO was used as negative control. The various microbial strains were subcultured and incubated at 37°C for 18-24 h to obtain young cultures and well-isolated colonies. These were then used to prepare inocula with a cell density cell density adjusted to 0.5 McFarland.

A swab was dipped into the tubes: tubes containing the inocula and then spread the contents over the entire surface of each dish containing Mueller-Hinton or Sabouraud media, ensuring even distribution of the inoculum. After being left at 4°C for 2 hours to allow dispersion, and 5 mm diameter wells were created and their bases sealed with soft agar.

The bases of the wells were sealed with soft agar. The wells were then

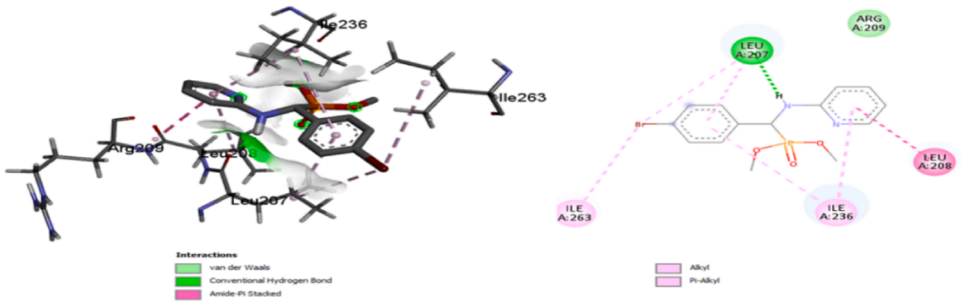

Fig. 11. Binding site structure of compound 3c- PqsR91-319.

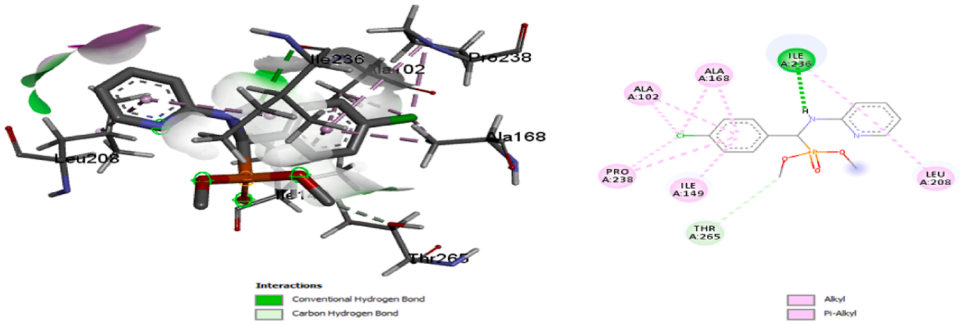

Fig. 12. Binding site structure of compound 3d- PqsR91-319.

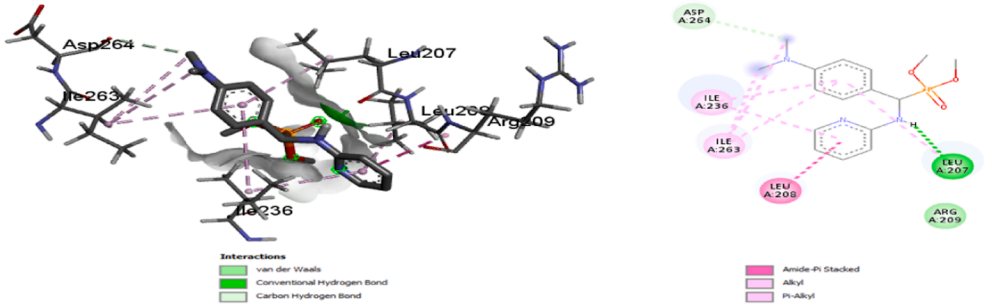

Fig. 13. Binding site structure of compound 3e- PqsR91-319.

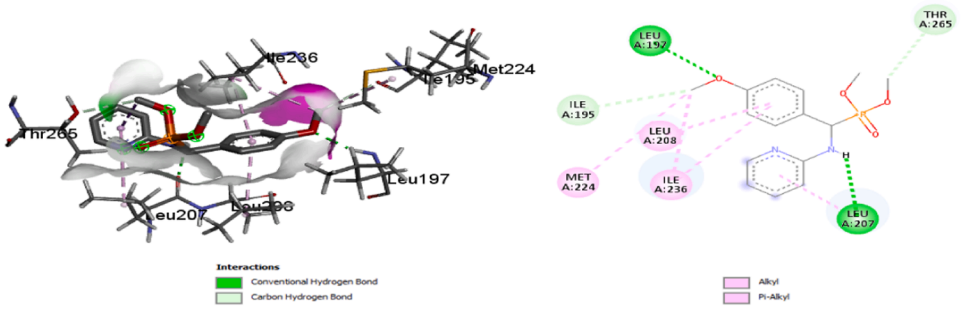

Fig. 14. Binding site structure of compound 3f- PqsR91-319.

filled with solutions of synthesized molecules. Plates were incubated at 37°C (bacteria) and 30°C (yeasts and fungi) for 48 hours. Antimicrobial activity was determined by measuring the diameter of the zone of inhibition, around the disc, against the test organism in millimeters. Experiments were carried out in triplicate, and the average diameter of the zone of inhibition was used.

3.3.3. Minimum inhibitory concentration (MIC)

MIC was estimated as the lowest concentration of antimicrobial agent which gave drop in OD600 equal to the medium negative control (below 0.05), after 24 h at 37°C of incubation.

It were determined using the broth microdilution method. as recommended by the National Committee for Clinical Laboratory Standards (NCCLS) [56].

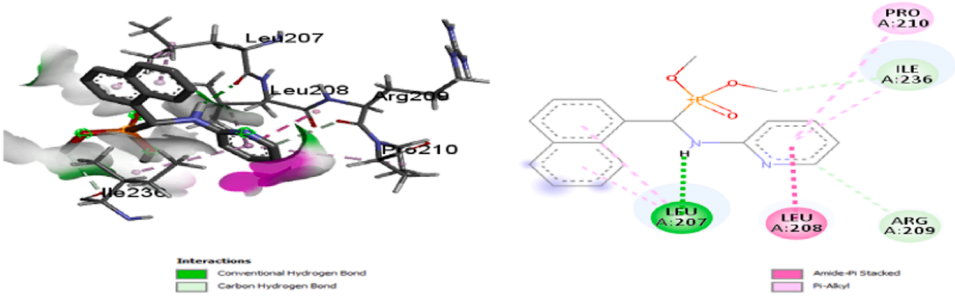

Fig. 15. Binding site structure of compound 3g- PqsR91-319.

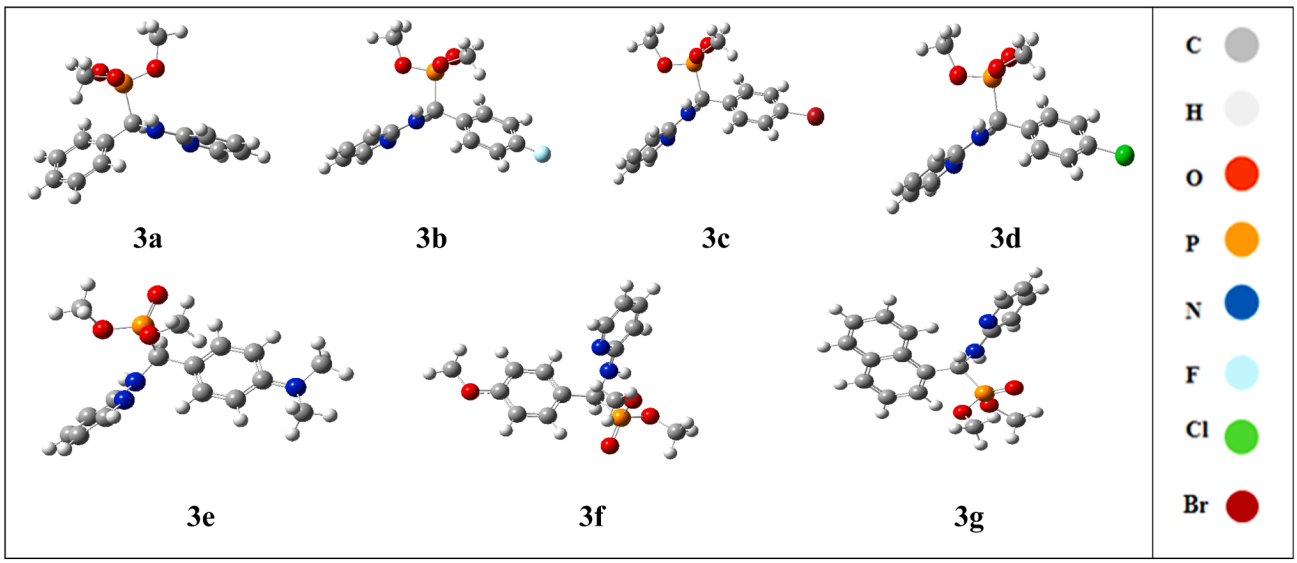

Fig. 16. Studied molecule's optimized structures by DFT B3LYP/6-31G (d,p).

Table 6
Global reactivity parameters equations.

Parameters	Equations
Ionisation energy	$I = -E_{HOMO}$
Electronic affinity	$A = -E_{LUMO}$
Electronégativity	$\chi = -(E_{HOMO} + E_{LUMO}) / 2$
Electronic chemical potential	$\mu = (E_{HOMO} + E_{LUMO}) / 2$
Chemical hardness	$\eta = (E_{LUMO} - E_{HOMO}) / 2$
Electrophilicity index	$\omega = \mu^2 / 2\eta$
molecular softness	$S = 1 / \eta$

MIC was estimated by the microtiter plate method using sterile 96-well plates Fifty microliters of these solutions were placed in the first row of microtiter plates.

Test compounds were diluted in DMSO in a series of two in sterile 96-well microtiter plates containing Mueller-Hinton broth (MHB) for Bacteria and Sabouraud broth for Yeast. A fresh culture of each microbial strain was used at a used at a volume of 100 µL for each well, after adjusting turbidity to 0.5 Mc Farland. Wells containing the inoculums alone were used as negative controls, and ampiclin and amphotericin b were used as positive controls. Microplates were incubated at 37°C for 24 hours.

MICs were determined at the concentrations corresponding to cups showing no microbial growth.

Infections with *Pseudomonas aeruginosa* (PA) are notoriously challenging to treat and often come with the development of antimicrobial resistance (AMR) [35].This resistance has become a global health concern, to the extent that the World Health Organization (WHO) has classified carbapenem-resistant Pseudomonas aeruginosa (PA) as one of

Table 7
Computed descriptors of titled compounds obtained by B3LYP / 6-31G (d,p).

Molecular Descriptors	3a	3b	3c	3d	3e	3f	3g
DM (D)	3.37	4.152	4.67	4.701	2.264	4.028	2.393
E_{HOMO} (eV)	- 5.638	- 5.724	- 5.778	- 5.777	- 4.998	- 5.523	- 5.511
E_{LUMO} (eV)	- 0.401	- 0.470	- 0.522	- 0.522	- 0.294	-0.439	-0.955
ΔE_{gap}(eV)	5.618	5.254	5.256	5.255	4.704	5.084	**4.556**
E (u.a)	- 1220.34	- 1319.56	- 3791.44	- 1679.93	- 1354.26	- 1334.85	- 1373.97
(η)	2.841	2.627	2.628	2.628	2.352	2.542	**2.278**
(*S*)	0.352	0.381	0.381	0.381	0.425	0.393	0.438
(µ)	- 3.042	- 3.097	- 3.150	- 3.149	- 2.646	- 2.981	- 3.233
(χ)	3.042	3.097	3.150	3.149	2.646	2.981	3.233
(ω)	1.628	1.825	1.887	1.886	1.488	1.726	**2.294**

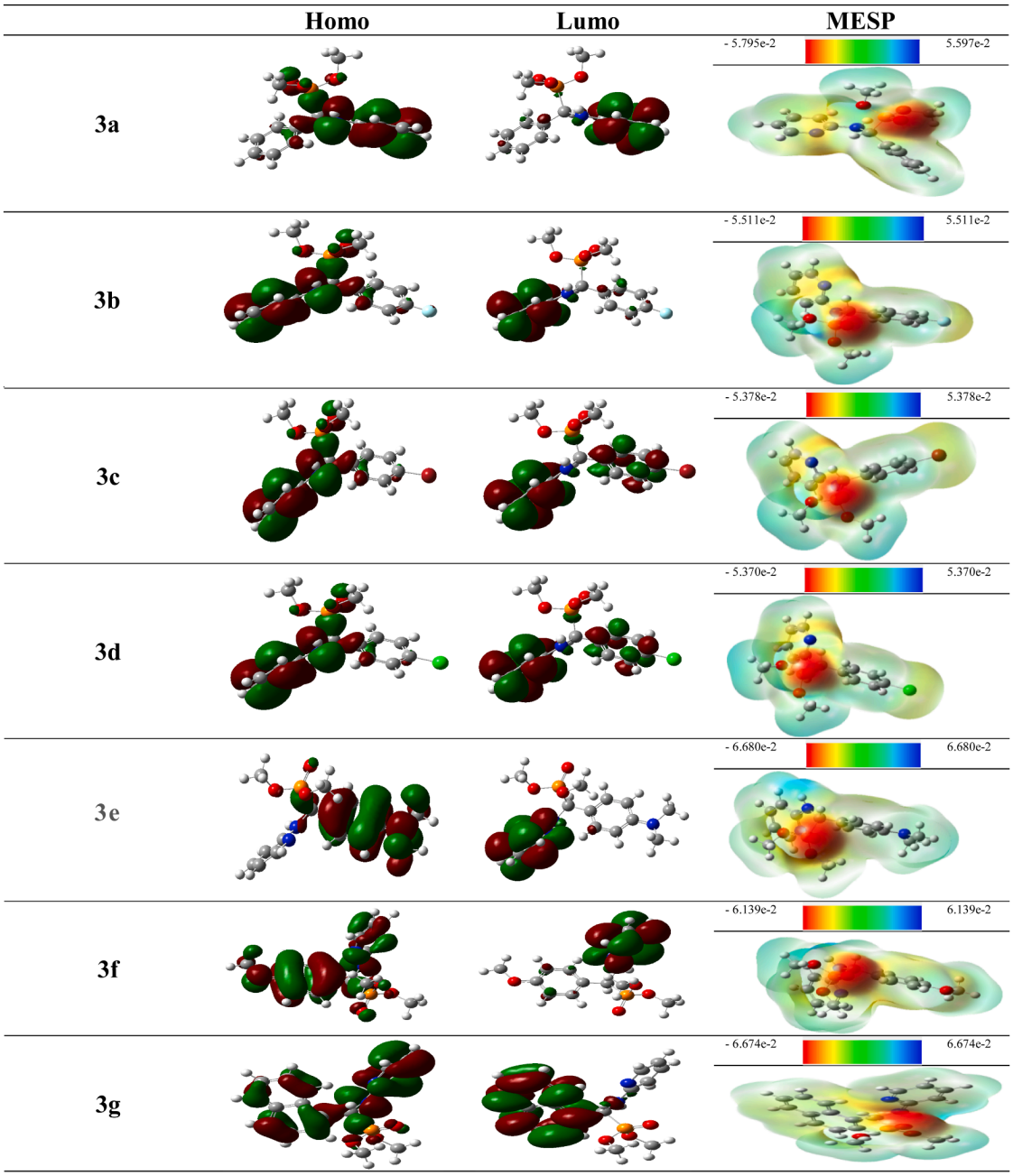

Fig. 17. Molecular electrostatic potential map on total density and levels energy (HOMO, LUMO) for titled compounds at B3LYP/6-31G (d,p) method.

Table 8
Principal experimental and calculated infrared frequency of compound **3g**.

Band	Experimental frequency ($\overline{\nu}_{exp}$) (cm^{-1})	Theoretical frequency ($\overline{\nu}_{exp}$) (cm^{-1})	$\Delta\overline{\nu}$ (cm^{-1})
NH	3297.68	3223.30	74.38
P=O	1233.37 cm^{-1}	1237.27	3.9
P-O	1050.12 cm^{-1}	1050.59	0.47
C=N	1603,74 cm^{-1}	1628.37	24.63

Table 9
Lipinski's five rules.

Characteristic	Requirement
Hydrogen bond donor	≤ 5
hydrogen bond receptor	< 10
molecular weight	< 500 Da
lipid water partition coefficient	< 5

the highest-priority pathogens to control.

3.4. Molecular docking study

3.4.1. Study protocol

The crystal structure of the quorum-sensing regulator MvfR (PqsR) downloaded from the protein data bank (PDB: 6YIZ) was selected as a receptor for docking study that were prepared and energetically minimized using the Protein Preparation wizard protocol of the Schrodinger Suite [57]. Molecular docking calculations were performed with AUTODOCK 4.2 [58] using the improved force field [59]. Autodock Tools were employed for identifying the torsion angles in the ligand, by adding the solvent model and assigning the Kollman atomic charges to

Table 10
Standard of drug's pharmacokinetic characteristics [38,39,45].

Characteristic	Requirement	Characteristic	Requirement
Polar (Polarity) $Å^2$	TPSA > 140	Flex [Flexibility]	0 < Num. rotatable bonds < 7
Insolu [Insolubility]	- 3.86< Log S (ESOL) < 2.05	Size ($g.mol^{-1}$)	126.20 < MW < 204.36
Water solubility partition coefficient	- 4.13 < log S <- 2.99	Log $P_{o/w}$ (iLOGP)	< 5

the protein. Ligand charges were calculated with the Gasteiger method. A grid spacing of 0.375 Å and a distance-dependent function of the dielectric constant were used for the energetic map calculations. The ligand were subjected to a robust docking procedure already used in virtual screening and pose prediction studies [60]. Each docked compound was subjected to 200 runs of the AUTODOCK search using the Lamarckian Genetic Algorithm performing 10 000 000 steps of energy evaluation. The number of individuals in the initial population was set to 500 and a maximum of 10 000 000 generations were simulated during each docking run. All other settings were left as their defaults and the best docked conformations were taken into account. For validation of

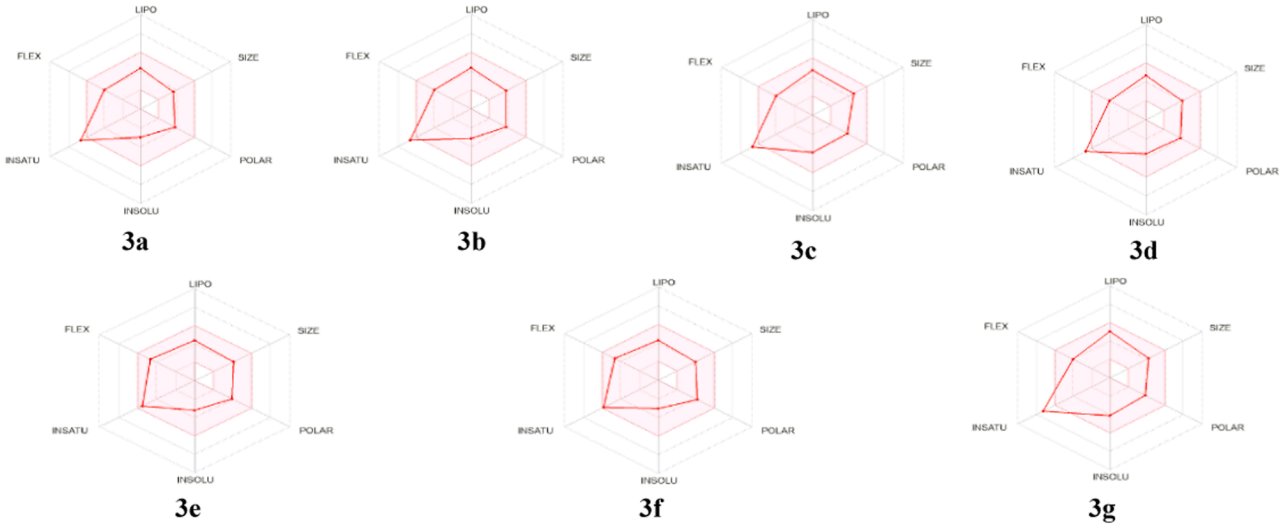

Fig. 18. Oral bioavailability radar of α-aminophosphonates studied compounds.

Table 11
α-aminophosphonates studied compounds' ADME proprieties.

	Molecular weight (g/mol)	Rotatable bonds	H-bond acceptors	H-bond donors	Violation LIPINSKI	Log $P_{o/w}$ (iLOGP)	Log *S* (ESOL)	GI absorption	BBB permeant	Log K_p cm/s	Bioavailability Score
3a	292.27	6	4	1	0	2.41	-2.99	High	Yes	-6.63	0.55
3b	310.26	6	5	1	0	2.60	-3.14	High	Yes	-6.67	0.55
3c	371.17	6	4	1	0	2.55	-3.89	High	Yes	-6.63	0.55
3d	326.72	6	4	1	0	2.36	-3.57	High	Yes	-6.40	0.55
3e	335.34	7	4	1	0	2.86	-3.21	High	Yes	-6.80	0.55
3f	322.30	7	5	1	0	2.52	-3.05	High	No	-6.84	0.55
3g	342.33	6	4	1	0	2.85	-4.13	High	Yes	-6.05	0.55

Table 12
Osiris calculations of studied compounds' toxicity risks.

compounds	Toxicity risks [a]				Osiris calculations [b]		
	MUT	TUM	IRRI	REP	TPSA	DL	DS
3a					70.26	- 26.6	0.16
3b					70.26	- 27.37	0.16
3c					70.26	- 28.67	0.14
3d					70.26	- 28.67	0.15
3e					82.29	- 27.52	0.10
3f					79.49	- 26.39	0.16
3g					70.26	- 27.02	0.04

Highly toxic: (■), Slightly toxic: (■), Not toxic: (■).

[a] **MUT** : Mutagenic, **TUM** : Tumorigenic, **IRRIT** : Irritant, **RE**: Reproductive effective. [b] **DL**: Drug-Likness, **DS**: Drug-Score, **TPSA** : Topological polar surface area.

the software the co-crystallized ligand was extracted and redocked into the active sites. To evaluate the quality of co-crystallized ligand, their Root Mean Square Deviation (RMSD) values were obtained. An RMSD value cut-of lesser than 2 Å is considered a good prediction for computed ligand-protein confirmation.

3.5. DFT study

The density functional theory (or DFT, for short) using B3LYP method [61,62] with 6- 31G (d,p) basis set has been employed to optimize the molecular structure of studied compounds by Gaussian 09 [63] and Gauss view molecular visualization program [64].

3.6. General procedure for the synthesis of a-aminophosphonate derivatives (3a–3g)

In an open glass tube (diameter: 25 mm; thickness: 1 mm; volume: 20 cm3) containing a mixture of 2-amino pyridine (1 equiv), trimethyl phosphite (1.2 equiv) and the respective aldehyde (1 equiv) at room temperature. The reaction was then sonicated by an ultrasonic bath at a frequency of 40 kHz for between 10 and 20 min. After completion of the reaction, after that, the solid product was recrystallized in diethyl ether and dried at room temperature in excellent yields; the precipitate was filtered and dried to obtain the final product.

The structure of the obtained α-aminophosphonate was confirmed by IR, RMN^{1}H, RMN ^{13}C, and RMN ^{31}P.

3.7. Spectroscopic data of the synthesized compounds

(*R, S*)-Dimethyl (phenyl(pyridin-2-ylamino)methyl)phosphonate 3a

White solid; yield 91%; m.p. 160-162°C;***^{1}H NMR (400 MHz, CDCl$_3$):*** d = 3.50 (d, J = 8 Hz, 3 H, OCH_3), 3.72 (d, J = 12 Hz, 3 H, OCH_3), 5.50-5.54 (t, J = 8 Hz, 1 H, NH), 5.58-5.66 (2d, J_1 = 8 Hz, J_2 = 12 Hz, 1 H, *CH), 6.34 (d, J = 8 Hz, 1H, $CH_{pyridin}$), 6.34 (t, J = 4 Hz, 1H, $CH_{pyridin}$), 7.26 (d, J = 8 Hz, 1H, $CH_{pyridin}$), 7.34 (m, 3 H, CH_{Ar}), 7.52 (d, 2H, CH_{Ar}), 8.06 (d, J = 4 Hz, 1H, $CH_{pyridin}$); ***RMN ^{13}C (100 MHz, CDCl$_3$)*** : δ= 51.37 (CH_3), 52.90 (CH_3), 53.67 (dd, J_{CP}= 5, 7 Hz, *CH), 108.63 (CH), 114.03 (CH), 128.00 (d, 2CH), 128.62 (d, 2CH), 136.07 (CH), 137.36 (CH), 147.97 (C), 156.81 (d, 2C) ppm; ***IR (KBr):*** 3301.35, 1227.35, 1021.93 cm^{-1}; ***RMN^{31}P (160 MHz, CDCl$_3$):*** δ= 25.00 ppm; ***Anal. Calc. for $C_{14}H_{17}N_2O_3P$:*** C, 57.51; H, 5.81; N, 9.58; O, 16.43; P, 10.61; ***Found:*** C, 57.53; H, 5.86; N, 9.58; O, 16.42; P, 10.60

(*R, S*)-Dimethyl ((4-fluorophényl)(pyridin-2-ylamino)methyl) phosphonate 3b

White solid; yield 90%; m.p. 181-183°C; ***^{1}H NMR (400 MHz, CDCl$_3$):*** d = 3.54 (d, J = 8 Hz, 3 H, OCH_3), 3.73 (d, J = 12 Hz, 3 H, OCH_3), 5.49-5.53 (t, J = 8 Hz, 1 H, NH), 5.58-5.66 (2d, J_1 = 8 Hz, J_2 = 4 Hz, 1 H, *CH), 6.34 (d, J = 12 Hz, 1H, $CH_{pyridin}$), 6.57-6.61 (t, J = 8 Hz, 1H, $CH_{pyridin}$), 7.00-7.04 (t, J = 8 Hz, 2H, CH_{Ar}), 7.34-7.38 (t, 1H, $CH_{pyridin}$), 7.49-7.35 (t, 2H, CH_{Ar}), 8.06 (d, J = 4 Hz, 1H, $CH_{pyridin}$); ***RMN ^{13}C (100 MHz, CDCl$_3$)*** : δ= 50.54, 52.07, 53.68 (dd), 108.76, 114.17, 115.54 (dd), 129.68 (dd), 137.40, 147.96, 156.63 (d), 161.22 (d) 163.67 (d) ppm; ***IR (KBr):*** 3264.29, 1217.02, 1026.33 cm^{-1}; ***RMN^{31}P (160 MHz, CDCl$_3$):*** δ= 25.05 ppm;; ***RMN ^{19}F (100 MHz, CDCl$_3$)*** : δ= -114 ppm; ***Anal. Calc. for $C_{14}H_{16}FN_2O_3P$* (310,09):** C, 54.17; H, 5.15; F, 6.12; N, 9.03; O, 15.48; P, 9.99; ***Found:*** C, 54.20; H, 5.20; F, 6.12; N, 9.03; O, 15.47; P, 9.98

(*R, S*)-Dimethyl ((4-bromophenyl)(pyridin-2-ylamino)methyl) phosphonate 3c

White solid; yield 90%; m.p. 178-180°C; ***^{1}H NMR (400 MHz, CDCl$_3$):*** d = 3.55-3.58 (d, J = 12 Hz, 3 H, OCH_3), 3.74-3.76 (d, J = 8 Hz, 3 H, OCH_3), 5.60-5. 69 (m, 2 H, NH + *CH), 6.45 (d, J = 8 Hz, 1H, $CH_{pyridin}$), 6.58-6.60 (t, J = 4 Hz, 1H, $CH_{pyridin}$), 7.29-7.38 (m, 3H, $CH_{pyridine}$+ CH_{Ar}), 7.47-7.49 (d, J = 8 Hz, 2H, CH_{Ar}), 8.05 (d, J = 4 Hz, 1H, $CH_{pyridin}$); ***RMN ^{13}C (100 MHz, CDCl$_3$)*** : δ= 50.63, 52.15, 53.73 (dd), 108.86, 114.18, 128.39 (d), 129.39 (d), 133.76(d), 134.87, 137.38, 147.91, 156.61 ppm; ***IR (KBr):*** 3299.15, 1230.17, 1025.85 cm^{-1}; ***RMN^{31}P (160 MHz, CDCl$_3$):*** δ= 24.80 ppm; ***Anal. Calc. for $C_{14}H_{16}BrN_2O_3P$* (370.01):** C, 45.40; H, 4.32; Br, 21.35; N, 7.56; O, 12.97; P, 8.64; ***Found:*** C, 45.30; H, 4.35; Br, 21.53; N, 7.55; O, 12.93; P, 8.34

(*R, S*)-Dimethyl ((4-chlorophenyl)(pyridin-2-ylamino)methyl) phosphonate 3d

White solid; yield 87%; m.p. 179-181°C;***^{1}H NMR (400 MHz, CDCl$_3$):*** d = 3.55-3.58 (d, J = 12 Hz, 3 H, OCH_3), 3.74-3.76 (d, J = 8 Hz, 3 H, OCH_3), 5.57-5. 68 (m, 2 H, NH + *CH), 6.44 (d, J = 8 Hz, 1H, $CH_{pyridin}$), 6.57-6.60 (t, J = 8 Hz, J = 4 Hz, 1H, $CH_{pyridin}$), 7.29-7.38 (m, 3H, $CH_{pyridine}$+ CH_{Ar}), 7.46-7.49 (d, J = 12 Hz, 2H, CH_{Ar}), 8.05 (d, J = 8 Hz, 1H, $CH_{pyridin}$); ***RMN ^{13}C (100 MHz, CDCl$_3$)*** : δ= 50.65, 52.18, 53.73 (dd), 108.84, 114.21, 128.76 (d), 129.38 (d), 133.78(d), 134.85, 137.40, 147.93, 156.59 ppm; ***IR (KBr):*** 3298.67, 1231.97, 1051.94 cm^{-1}; ***RMN^{31}P (160 MHz, CDCl$_3$):*** δ= 24.84 ppm; ***Anal. Calc. for $C_{14}H_{16}ClN_2O_3P$* (326,06):** C, 51.52; H, 4.90; Cl, 10.88; N, 8.58; O, 14.72; P, 9.81; ***Found:*** C, 51.47; H, 4.94; Cl, 10.85; N, 8.57; O, 14.69; P, 9.48

(*R, S*)-Dimethyl ((4-(dimethylamino)phenyl)(pyridin-2-ylamino)methyl)phosphonate 3e

White solid; yield 73%; m.p. 166-168°C; ***^{1}H NMR (400 MHz, CDCl$_3$):*** s = 2.92 (s, 6H, $2CH_3$), d = 3.51 (d, J = 8 Hz, 3 H, OCH_3), 3.72 (d, J = 8 Hz, 3 H, OCH_3), 5.36-5.38 (t, J = 4 Hz, 1 H, NH), 5.42-5.49 (2d, J= 8 Hz, 1 H, *CH), 6.40 (d, J = 8 Hz, 1H, $CH_{pyridin}$), 6.56 (t, J = 8 Hz, 1H, $CH_{pyridin}$), 6.67 (d, J = 12 Hz, 2H, CH_{Ar}), 35-7.38 (m, 1H, $CH_{pyridin}$, 2H CH_{Ar}), 8.07 (d, J = 4 Hz, 1H, $CH_{pyridin}$), 7; ***RMN ^{13}C (100 MHz, CDCl$_3$)*** : δ= 40.43, 50.86, 52.41 (dd), 53.61 (dd), 108.48, 112.51(d), 113.83, 123.10, 128.81 (d), 137.32, 147.98, 150.27 (d) 157.01 (d) ppm; ***IR (KBr):*** 3291.07, 1232.80, 1062.15 cm^{-1}; ***RMN^{31}P (160 MHz, CDCl$_3$):*** δ= 25.77 ppm; ***Anal. Calc. for $C_{16}H_{22}N_3O_3P$* (335,14):** C, 57.28; H, 6.56; N, 12.53; O, 14.32; P, 9.25; ***Found:*** C, 57.31; H, 6.61; N, 12.53; O, 14.31; P, 9.24

(*R, S*)-Diméthyl ((4-methoxyphenyl)(pyridin-2-ylamino) methyl)phosphonate 3f

White solid; yield 88%; m.p. 158-160°C; ***^{1}H NMR (400 MHz, CDCl$_3$):*** d = 3.51 (d, J = 12 Hz, 3H,P OCH_3), 3.72 (d, J = 8 Hz, 3 H,P OCH_3), s = 3.72 (s, 3H, OCH_3), 5.41-5.45 (t, J = 8 Hz, 1H, NH), 5.50-5.58 (2d, J= 12 Hz, J= 24 Hz, 1 H, *CH), 6.41 (d, J = 8 Hz, 1H, $CH_{pyridin}$), 6.56 (t, J = 8 Hz, 1H, $CH_{pyridin}$), 6.86 (d, J = 12 Hz, 2H, CH_{Ar}), 7.34 (t, J = 12Hz, 3H, $CH_{pyridin}$), 7.43 (d, J = 12 Hz, 2H, CH_{Ar}), 8.07 (d, J = 4 Hz, 1H, $CH_{pyridin}$); ***RMN ^{13}C (100 MHz, CDCl$_3$)*** : δ= 50.73, 52.27, 53.46 (dd), 55.23, 108.59, 114.06(m), 127.97, 129.17 (d), 137.35, 147.98, 156.85 (d) 159.35 (d) ppm; ***IR (KBr):*** 3303.30, 1229.02, 1027.44 cm^{-1}; ***RMN^{31}P (160 MHz, CDCl$_3$):*** δ= 25.32 ppm; ***Anal. Calc. for $C_{15}H_{19}N_2O_4P$* (322,11):** C, 55.88; H, 5.89; N, 8.69; O, 19.86; P, 9.93; ***Found:*** C, 55.90; H, 5.94; N, 8.69; O, 19.86; P, 9.61

(*R, S*)-Dimethyl (naphthalen-1-yl(pyridin-2-ylamino)methyl) phosphonate 3g

White solid; yield 70%; m.p. 158-160°C;***^{1}H NMR (400 MHz, CDCl$_3$):*** d = 3.48 (d, J = 12 Hz, 3H, OCH_3), 3.74 (d, J = 12 Hz, 3 H, OCH_3), s = 3.72 (s, 3H, OCH_3), 5.58-5.61 (t, J = 8 Hz, 1H, NH), 5.72-5.80 (2d, J= 8 Hz, 1 H, *CH), 6.47-8.53 (m, 11H, CH_{napht}+ $CH_{pyridin}$); ***RMN ^{13}C (100 MHz, CDCl$_3$)*** : δ= 51.66, 53.18, 53.47, 108.57, 114.02, 119.88, 121.88, 124.23, 126.62, 127.87(d), 128.99, 132.47, 137.71, 138.17, 148.17, 148.93, 162.90 ppm; ***IR (KBr):*** 3297.68, 1233.37, 1050.12 cm^{-1}; ***RMN^{31}P (160 MHz, CDCl$_3$):*** δ= 25.20 ppm; ***Anal. Calc. for $C_{18}H_{19}N_2O_3P$* (342,11):** C, 63.13; H, 5.55; N, 8.18; O, 14.03; P, 9.35; ***Found:*** C, 63.15; H, 5.59; N, 8.18; O, 14.02; P, 9.05.

4. Conclusions

In conclusion, in the present work, we report the synthesis, crystallographic, biological, docking analysis and computational studies of the new α-aminophosphonates. The target compounds were obtained by a

simple and efficient multicomponent Kabachnik-Field reaction from 2-amino pyridine, various aldehydes and trimethylphosphite. The structures of the newly synthesized compounds were determined based on usual spectroscopic data (IR, ^{1}H-NMR, ^{13}C-NMR, ^{31}P-NMR). In addition, an X-ray diffraction analysis was performed on the single crystals of compound **3g** further confirms the structure of the target molecules. The compounds **3a-d** and **3f** were evaluated for their antimirobial activity. The tested compounds have excellent antibacterial effects against the different strains tested, ranging from 14 to 34 mm diameter of inhibition zone a MIC of 32 to 128 μg/mL. Furthermore, a docking study was conducted on the targeted compounds to corroborate the experimental findings. The results revealed a notably high docking score and favorable binding energy with the target enzyme. When compared to the reference ligand, the investigated compounds exhibited superior docking scores and binding free energies.

CRediT authorship contribution statement

Ismahene Grib: Methodology. **Malika Berredjem:** Writing – review & editing. **Seif-Eddine Djouad:** Validation. **Chahrazed Benzaid:** Investigation. **Khadidja Otmane Rachedi:** Conceptualization. **Rania Bahadi:** Investigation. **Lina Manel Djendi:** Formal analysis. **Malika Ibrahim-Ouali:** Formal analysis. **Sofiane Bouacida:** Formal analysis. **Khaldoun Bachari:** Formal analysis. **Yacine Laichi:** Formal analysis. **Christelle Marminon:** Supervision. **Marc LE Borgne:** Supervision. **Radia Bouasla:** Visualization.

Declaration of competing interest

The authors declare that they have no known competing financial interests or personal relationships that could have appeared to influence the work reported in this paper.

Data availability

No data was used for the research described in the article.

Acknowledgments

This work was supported financially by The General Directorate for Scientific Research and Technological Development (DG-RSDT), Algerian Ministry of Scientific Research.

References

[1] L. Berlicki, P. Kafarski, Computer-aided analysis and design of phosphonic and phosphinic enzyme inhibitors as potential drugs and agrochemicals, Curr. Org. Chem. 9 (2005) 1829–1850, https://doi.org/10.2174/138527205774913088.

[2] M. Sieńczyk, Ł. Winiarski, P. Kasperkiewicz, M. Psurski, J. Wietrzyk, J. Oleksyszyn, Simple phosphonic inhibitors of human neutrophil elastase, Bioorg. Med. Chem. Lett. 21 (2011) 1310–1314, https://doi.org/10.1016/j.bmcl.2011.01.083.

[3] S. Vassiliou, E. Węglarz-Tomczak, Ł. Berlicki, M. Pawełczak, B. Nocek, R. Mulligan, A. Joachimiak, A. Mucha, Structure-guided, single-point modifications in the phosphinic dipeptide structure yield highly potent and selective inhibitors of neutral aminopeptidases, J. Med. Chem. 57 (2014) 8140–8151, https://doi.org/10.1021/jm501071f.

[4] T. Arya, R. Reddi, C. Kishor, R.J. Ganji, S. Bhukya, R. Gumpena, S. McGowan, M. Drag, A. Addlagatta, Identification of the molecular basis of inhibitor selectivity between the human and streptococcal type i methionine aminopeptidases, J. Med. Chem. 58 (2015) 2350–2357, https://doi.org/10.1021/jm501790e.

[5] M.V.N. Reddy, A. Balakrishna, M.A. Kumar, G.C.S. Reddy, A.U.R. Sankar, C. S. Reddy, T.M. Krishna, One-step synthesis and bioassay of N-phosphoramidophosphonates, Chem. Pharm. Bull. 57 (2009) 1391–1395, https://doi.org/10.1248/cpb.57.1391.

[6] J.Y. Che, X.Y. Xu, Z.L. Tang, Y.C. Gu, D.Q. Shi, Synthesis and herbicidal activity evaluation of novel α-amino phosphonate derivatives containing a uracil moiety, Bioorg. Med. Chem. Lett 26 (2016) 1310–1313, https://doi.org/10.1016/j.bmcl.2016.01.010.

[7] S.A. Dake, D.S. Raut, K.R. Kharat, R.S. Mhaske, S.U. Deshmukh, R.P. Pawar, Ionic liquid promoted synthesis, antibacterial and in vitro antiproliferative activity of novel α-aminophosphonate derivatives, Bioorg. Med. Chem. Lett 21 (2011) 2527–2532, https://doi.org/10.1016/j.bmcl.2011.02.039.

[8] M.R. Sivala, S.R. Devineni, M. Golla, V. Medarametla, G.K. Pothuru, N. R. Chamarthi, heterogeneous catalyst, SiO_2 -$ZnBr_2$: an efficient neat access for α-aminophosphonates and antimicrobial activity evaluation, J. Chem. Sci 128 (2016) 1303–1313, https://doi.org/10.1007/s12039-016-1113-1.

[9] K.U.M. Rao, S. Swapna, D.M. Manidhar, K.M.K. Reddy, C.S. Reddy, Efficient synthesis of α-aminophosphonates and evaluation of significance of PO group towards antioxidant activity Phosphorus Sulfur Silicon Relat, Elem 190 (2015) 232–239, https://doi.org/10.1080/10426507.2014.914937.

[10] M. Cassien, C. Petrocchi, S. Thétiot-Laurent, M. Robin, E. Ricquebourg, C. Kandouli, A. Asteian, A. Rockenbauer, A. Mercier, M. Culcasi, S. Pietri, On the vasoprotective mechanisms underlying novel β-phosphorylated nitrones: Focus on free radical characterization, scavenging and NO-donation in a biological model of oxidative stress, Eur. J. Med. Chem. 119 (2016) 197–217, https://doi.org/10.1016/j.ejmech.2016.04.067.

[11] a) P. Clezardin, Bisphosphonates' antitumor activity: an unravelled side of a multifaceted drug class, Bone 48 (2011) 71–79, https://doi.org/10.1016/j.bone.2010.07.016;
b) Servier Medical Art. Neuilly-sur-Seine, Les Laboratoires Servier, France, 2006 [updated 14.01.08; accessed 11.03.11];
c) J. Green, P. Clezardin, The molecular basis of bisphosphonate activity: a preclinical perspective, Semin. Oncol. 37 (2010) S3–S11, https://doi.org/10.1053/j.seminoncol.2010.06.003.

[12] a) X.C. Huang, M. Wang, Y.M. Pan, X.Y. Tian, H.S. Wang, Y. Zhang, Synthesis and antitumor activities of novel α-aminophosphonates dehydroabietic acid derivatives, Bioorg. Med. Chem. Lett. 23 (2013) 5283, https://doi.org/10.1016/j.bmcl.2013.08.005;
b) M. Berredjem, A. Bouzina, R. Bahadi, S. Bouacida, V. Rastija, D. Seif-Eddine, T. O. Sothea, F. Almalki, T. Hadda, M. Aissaoui, Antitumor activity, X-Ray crystallography, in silico study of some-sulfamido-phosphonates. Identification of pharmacophore sites, J. Mol. Struct 1250 (2022) 131886, https://doi.org/10.1016/j.molstruc.2021.131886.

[13] J. Tian, R. Ji, H. Wang, S. Li G. Zhang, Discovery of novel α-aminophosphonates with hydrazone as potential antiviral agents combined with active fragment and molecular docking, Front. Chem. 10 (2022) 911453, https://doi.org/10.3389/fchem.2022.911453.

[14] S.A.R. Mulla, M.Y. Pathan, S.S. Chavan, S.P. Gample, D Sarkar, Highly efficient one-pot multi-component synthesis of α-aminophosphonates and bis-α-aminophosphonates catalyzed by heterogeneous reusable silica supported dodecatungstophosphoric acid (DTP/SiO2) at ambient temperature and their antitubercular evaluation against Mycobactrium Tuberculosis, RSC. Adv. 4 (2014) 7666, https://doi.org/10.1039/C3RA45853A.

[15] F Bouchareb, M Berredjem, Recent progress in the synthesis of phosphoramidate and phosphonamide derivatives: a review, Phosphorus. Sulfur. Silicon. Relat. Elem. 197 (2022) 711–731, https://doi.org/10.1080/10426507.2021.2012781.

[16] G.S. Reddy, K.U.M. Rao, C.S. Sundar, S.S. Sudha, B.i Haritha, S. Swapna, C. S. Reddy, Neat synthesis and antioxidant activity of α-aminophosphonates, Arab. J. Chem. 7 (2014) 833–838, https://doi.org/10.1016/j.arabjc.2013.01.004.

[17] M.K. Awad, M.F. Abdel-Aal, F.M. Atlam, H.A. Hekal, Molecular docking, molecular modeling, vibrational and biological studies of some new heterocyclic α-aminophosphonates, J. Mol. Struct. 1173 (2018) 128, https://doi.org/10.1016/j.saa.2018.07.083.

[18] D.A Elsherbiny, A.M. Abdelrahman, E.M. El-Naggar, R.A. El-Sherbiny, M.H. El-Rafie, I.E. El-Tantawy El-Sayed, Synthesis, antimicrobial activity, and sustainable release of novel α-aminophosphonate derivatives loaded carrageenan cryogel, Int. J. Biol. Macromol. 163 (2020) 107, https://doi.org/10.1016/j.ijbiomac.2020.06.251.

[19] R. Redjemia, M Berredjem, R Bahadi, Green and cost-effective synthesis of sulfamidophosphonates using ZnO nanoparticles as catalyst, Eng. Proc. 37 (2023) 98, https://doi.org/10.3390/ECP2023-14733.

[20] R Bahadi, M Berredjem, C Benzaid, F Bouchareb, A Dekir, ML Djendi, M. Ibrahim-Ouali, M. Boussaker, S. Bouacida, A.R. Bhat, S. Ahmed, K. Bachari, R. Redjemia, Efficient synthesis, crystallography study, antibacterial/antifungal activities, DFT/ADMET studies and molecular docking of novel α-aminophosphonates, J. Mol. Struct 1289 (2023) 135849, https://doi.org/10.1016/j.molstruc.2023.135849.

[21] S.E. Djouad, M. Berredjem, F.Z. Hadjadj Aoul, F. Bouchareb, M. Guerfi, T. Ben Hadda, M. Aissaoui, B. Belhani, In silico drug design and molecular docking of novel amidophosphonates and sulfamidophosphonates as inhibitors of urokinase-type plasminogen activator, J. Indian Chem. Soc 99 (2022) 100650, https://doi.org/10.1016/j.jics.2022.100650.

[22] R. Bahadi, R. Boughoula, M. Berredjem, K. Bachari, A. Bouzina, S. Bouacida, H. Sbartai, F Benalliouche, R. Redjemia, A convenient synthesis, biological activity and X-ray crystallography of novel α-aminophosphonate derivatives, Phosphorus Sulfur Silicon Relat. Elem. 197 (2022) 1150–1156, https://doi.org/10.1080/10426507.2022.2064859.

[23] I. Grib, B. Belhani, K. Bechlem, R. Bouasla, N. Aouf, M. Berredjem, Ultrasonic assisted green protocol for the synthesis of sulfamides, Phosphorus Sulfur Silicon Relat. Elem. 192 (2017) 827–830, https://doi.org/10.1080/10426507.2017.1287184.

[24] I. Grib, A. Bouzina, N.E. Aouf, M. Berredjem, A practical and green approach towards synthesis of new N-sulfonylimines under ultrasound irradiation, Phosphorus Sulfur Silicon Relat. Elem. 191 (2016) 1086–1091, https://doi.org/10.1080/10426507.2016.1138306.

[25] I. Grib, M. Berredjem, K. Otmane Rachedi, S.E. Djouad, S. Bouacida, R. Bahadi, Tan-Sothea Ouk, M. Kadri, T. Ben Hadda, B. Belhani, Novel N-sulfonylphthalimides: Efficient synthesis, X-ray characterization, spectral investigations, POM analyses, DFT computations and antibacterial activity, J. Mol. Struct 1217 (2020) 128423, https://doi.org/10.1016/j.molstruc.2020.128423.

[26] F. Bouchareb, M. Berredjem, A. Bouzina, M. Guerfi, Ultrasound-promoted, rapid and green synthesis of phosphonamide derivatives under catalyst and solvent-free conditions, Phosphorus Sulfur Silicon Relat. Elem. 196 (2021) 422–430, https://doi.org/10.1080/10426507.2020.1854254.

[27] M.C. Burla, R. Caliandro, M. Camalli, B. Carrozzini, G.L. Cascarano, L. De Caro, C. Giacovazzo, G. Polidori, R. Spagna, an improved tool for crystal structure determination and refinement, J. Appl. Cryst. 38 (2005) 381–388, https://doi.org/10.1107/S002188980403225X.

[28] V.G. de Billerbeck, Huiles essentielles et Bactéries Résistantes Aux Antibiotiques, 5, Springer Link, Phytothérapie, 2007, pp. 249–253, https://doi.org/10.1007/s10298-007-0265-z.

[29] Benzaid C, L. Tichati, M. Rouabhia, S. Akil Dahdouh, Prevalence of microbial nosocomial infections in the resuscitation unit of the University Hospital of Annaba-Algeria, Ann Biol Clin 6 (2022) 80, https://doi.org/10.1684/abc.2022.1766.

[30] R. Leclercq, V. Cattoir, Bactéries à Gram positif et glycopeptides, Rev. Francophone Lab. (2012) 41–46, https://doi.org/10.1016/S1773-035X(12)71675-1, 2012.

[31] C. Schütz, D. Ho, M.M. Hamed, A.S. Abdelsamie, T. Röhrig, C. Herr, M. Empting, A new PqsR inverse agonist potentiates tobramycin efficacy to eradicate pseudomonas aeruginosa biofilms, Adv. Sci. 8 (2021) 2004369, https://doi.org/10.1002/advs.202004369.

[32] S. Wagner, R. Sommer, S. Hinsberger, C. Lu, R.W. Hartmann, M. Empting, A. Titz, Novel strategies for the treatment of pseudomonas aeruginosa infections, J. Med. Chem 59 (2016) 5929–5969, https://doi.org/10.1021/acs.jmedchem.5b01698.

[33] M.F Noirot-Gros, S. Forrester, G. Malato, P.E. Larsen, P. Noirot, CRISPR interference to interrogate genes that control biofilm formation in Pseudomonas fluorescens, Sci. Rep. 9 (2019) 15954, https://doi.org/10.1038/s41598-019-52400-5.

[34] A. Thomann, A.G.G. de Mello Martins, C. Brengel, M. Empting, R.W. Hartmann, Application of Dual Inhibition Concept within Looped Autoregulatory Systems toward Antivirulence Agents against Pseudomonas aeruginosa Infections, ACS. Chem. Biol. 11 (2016) 1279–1286, https://doi.org/10.1021/acschembio.6b00117.

[35] C. Schütz, D.K. Ho, M.M. Hamed, A.S. Abdelsamie, T. Röhrig, C. Herr, A new PqsR inverse agonist potentiates tobramycin efficacy to eradicate Pseudomonas aeruginosa biofilms, Adv. Sci. 8 (12) (2021) 2004369, https://doi.org/10.1002/advs.202004369.

[36] R. Redjemia, M. Berredjem, A. Dekir, M.I. Ouali, M. Aissaoui, S. Bouacida, A. Bouzina, R. Bahadi, A convenient synthesis, in silico study and crystal structure of novel sulfamidophosphonates: Interaction with SARS-CoV-2, J. Mol. Struct. 1275 (2023) 134602, https://doi.org/10.1016/j.molstruc.2022.134602.

[37] A.R. Bhat, R.S. Dongre, F.A. Almalki, M. Berredjem, M. Aissaoui, R. Touzani, T. Ben Hadda, M.S. Akhter, Synthesis, biological activity and POM/DFT/docking analyses of annulated pyrano [2,3d]pyrimidine derivatives: identification of antibacterial and antitumor pharmacophore sites, Bioorg. Chem. 106 (2021) 104480, https://doi.org/10.1016/j.bioorg.2020.104480.

[38] A. Khaled, R. Kadri, M. Kadri, M. Berredjem, New Cu (II) and Zn(II) complexes with diethyl phenyl (N-phenylsulfamoylamino) methyl phosphonate: synthesis, characterisation, DFT/M11 studies, NBO, DOS, QTAIM and RDG analysis, J. Mol. Struct. 1263 (2022) 133003–133016, https://doi.org/10.1016/j.molstruc.2022.133003.

[39] H. Lafridi, F.A. Almalki, T. Ben Hadda, M. Berredjem, M.A. Kawsar, A. M. Alqahtani, E.R. Esharkawy, B. Lakhrissi, H. Zgou, In silico evaluation of molecular interactions between macrocyclic inhibitors with the HCV NS3 protease. Docking and identification of antiviral pharmacophore site, J. Biomol. Struct. Dyn. 41 (2023) 2260–2273, https://doi.org/10.1080/07391102.2022.2029571.

[40] K.O. Rachedi, R. Bahadi, M. Aissaoui, T.B. Hadda, B. Belhani, A. Bouzina, DFT Study, POM analyses and molecular docking of novel oxazaphosphinanes: Identification of antifungal pharmacophore site, Indones. J. chem. 20 (2020) 440–450, https://doi.org/10.22146/ijc.46375.

[41] P. Senet, Chemical hardnesses of atoms and molecules from frontier orbitals, Chem. Phys. Lett. 275 (1997) 527–532, https://doi.org/10.1016/S0009-2614(97)00799-9.

[42] R.G. Parr, R.G. Pearson, Absolute hardness: companion parameter to absolute electronegativity, J. Am. Chem. Soc. 105 (1983) 7512–7516, https://doi.org/10.1021/ja00364a005.

[43] L. Pauling, The Nature of the Chemical Bond, Cornell University Press, Ithaca, NY, USA, 1960.

[44] W. Boufas, N. Dupont, M. Berredjem, K. Berrezag, I. Becheker, H. Berredjem, N. E. Aouf, Synthesis and antibacterial activity of sulfonamides. SAR and DFT studies, J. Mol. Struct. 1074 (2014) 180–185, https://doi.org/10.1016/j.molstruc.2014.05.066.

[45] D. Antoine, M. Olivier, Z. Vincent, SwissADME: a free web tool to evaluate pharmacokinetics, drug-likeness and medicinal chemistry friendliness of small molecules, Sci. Rep. 7 (2017) 42717, https://doi.org/10.1038/srep42717.

[46] D. Antoine, Z. Vincent, A BOILED-Egg to predict gastrointestinal absorption and brain penetration of small molecule, Chem. Med. Chem. 11 (2016) 1117–1121, https://doi.org/10.1002/cmdc.201600182.

[47] C.A. Lipinski, Drug-like properties and the causes of poor solubility and poor permeability, J. Pharmacol. Toxicol. Methods 44 (2000) 235–249, https://doi.org/10.1016/s1056-8719(00)00107-6.

[48] C.A. Lipinski, B.W.Dominy F.Lombardo, P.J. Feeney, Experimental and computational approaches to estimate solubility and permeability in drug discovery and development settings, Adv. Drug Deliv. Rev. 46 (1-3) (2001) 3–26, https://doi.org/10.1016/S0169-409X(00)00129-0.

[49] https://www.organic-chemistry.org/prog/peo/.

[50] M.M. da Silva, M. Comin, T.S. Duarte, M.A. Foglio, J.E. De Carvalho, M.D. Vieira, A.S.N. Formagio, Synthesis, antiproliferative activity and molecular properties predictions of galloyl derivatives, Molecules. 20 (2015) 5360–5373, https://doi.org/10.3390/molecules20045360.

[51] M.C. Burla, R. Caliandro, M. Camalli, B. Carrozzini, G.L. Cascarano, L. De Caro, C. Giacovazzo, G. Polidori, R. Spagna, SIR2004: an improved tool for crystal structure determination and refinement, J. Appl. Cryst 38 (2005) 381–388, https://doi.org/10.1107/S002188980403225X.

[52] G.M. Sheldrick, A short history of SHELX, Acta Cryst. 64 (2008) 112–122, https://doi.org/10.1107/S0108767307043930.

[53] L.J. Farrugia, WinGX and ORTEP for Windows: an update, J. Appl. Cryst 45 (2012) 849–854, https://doi.org/10.1107/S0021889812029111.

[54] K. Brandenburg, M. Berndt, DIAMOND Version 2.1. Crystal Impact, 2001.

[55] C. Benzaid, L. Lazhari Tichati, R. Djeribi, M. Rouabhia, Evaluation of the chemical composition, the antioxidant and antimicrobial activities of mentha × piperita essential oil against microbial growth and biofilm formation, J. Essent. Oil Bear. PL 22 (2019) 335–346, https://doi.org/10.1080/0972060X.2019.1622456.

[56] National Committee for Clinical Laboratory Standards, Methods for dilution antimicrobial susceptibility tests for bacteria that grow aerobically, in: Approved Standard NCCLS Document M7-A6, 6th ed., 23, NCCLS, Wayne, PA, USA, January 2003. No. 2.

[57] G. Madhavi Sastry, M. Adzhigirey, T. Day, R. Annabhimoju, W. Sherman, Protein and ligand preparation: parameters, protocols, and influence on virtual screening enrichments, J. Comput. Aided. Mol. Des. 27 (2013) 221–234, https://doi.org/10.1007/s10822-013-9644-8.

[58] G.M. Morris, D.S. Goodsell, R.S. Halliday, R. Huey, W.E. Hart, R.K. Belew, A. J. Olson, Automated docking using a Lamarckian genetic algorithm and an empirical binding free energy function, J. Comput. Chem. 19 (1998) 1639–1662, https://doi.org/10.1002/(sici)1096-987x(19981115)19:14≤1639::aid-jcc10≥3.0.co;2-b.

[59] D. Santos-Martins, S. Forli, M.J. Ramos, A.J. Olson, AutoDock4Zn: an improved AutoDock force field for small-molecule docking to zinc metalloproteins, J. Chem. Inf. Model. 54 (2014) 2371–2379, https://doi.org/10.1021/ci500209e.

[60] G. Poli, A. Gelain, F. Porta, A. Asai, A. Martinelli, T. Tuccinardi, Identification of a new STAT3 dimerization inhibitor through a pharmacophore-based virtual screening approach, J. Enzyme Inhib. Med. Chem. 31 (2015) 1011–1017, https://doi.org/10.3109/14756366.2015.1079184.

[61] A.B. Becke, Density-functional thermochemistry. III. The role of exact exchange, J. Chem. Phys. 98 (1993) 5648–5652, https://doi.org/10.1063/1.464913.

[62] M.M. Francl, W.J. Pietro, W.J. Hehre, J.S. Binkley, M.S. Gordon, D.J. De Frees, J. A. Pople, Self-consistent molecular orbital methods. XXIII. A polarization-type basis set for second-row elements, J. Chem. Phys 77 (1982) 3654–3665, https://doi.org/10.1063/1.444267.

[63] M. Frisch, G. Trucks, H. Schlegel, G. Scuseria, M. Robb, J. Cheeseman, G. Scalmani, V. Barone, B. Mennucci, G. Petersson, Gaussian 09, 32, Gaussian, Inc, Wallingford, CT, 2009, pp. 5648–5652.

[64] Æ. Frisch, H. P. Hratchian, R. D. Dennington II, T. A. Keith, J. Millam, A. B. Nielsen, A. J. Holder, J. Hiscocks. Gaussian, Inc. 340 Quinnipiac Street, Building 40 Wallingford, CT 06492 USA.